

MORPHO-STRUCTURAL MODIFICATIONS USING THERMAL TREATMENTS ON IRON OXIDE NANOPARTICLES SYNTHESIZED BY LASER PYROLYSIS USING FORMIC ACID AS A SENSITIZER

A. CRIVEANU¹, F. DUMITRACHE¹, I. LUNGU¹, I.P. MORJAN¹, L. GAVRILA¹, C. FLEACA¹, A. BANICI¹, A. BALAN², R. M. DUMITRACHE², V. SOCOLIUC^{3,4}, B. VASILE^{5,6}

¹ National Institute for Laser, Plasma and Radiation Physics, 409 Atomistilor St., 077125 Magurele, Romania;

² The Faculty of Physics, University Bucharest, 077125 Bucharest, Romania;

³ Romanian Academy - Timisoara Branch, Center for Fundamental and Advanced Technical Research, Laboratory for Magnetic Fluids, 24 Mihai Viteazu Ave., 300223 Timisoara, Romania

⁴ Research Center for Complex Fluids Systems Engineering, Politehnica University of Timisoara, 1 M. Viteazu Ave., 300222 Timisoara, Romania

⁵ Advanced Research Center for Innovative Materials, Products and Processes National University of Science and Technology POLITEHNICA Bucharest, Splaiul Independentei 313, 060042 Bucharest, Romania;

⁶ Academy of Romanian Scientists, 3 Ilfov, 050044 Bucharest, Romania

Corresponding author, Email: florian.dumitrache@infpr.ro

Keywords: iron oxide nanoparticles; laser pyrolysis; formic acid;

The laser pyrolysis technique was used in the synthesis of magnetic iron oxide nanopowders (NPs) in the presence of formic acid vapors as a sensitizer. This technique uses the energy from a continuous-wave CO₂ laser operating at a 9.25 μm wavelength, which is transferred to the reactive precursors via a resonant absorption of formic acid molecules. The iron precursor-Fe(CO)₅ and the sensitizer (H-COOH) vapors were obtained by bubbling an argon flow, through the liquid reservoirs. The laser irradiation of reactive gas mixture induces a rapid heating and followed by a decomposition of the Fe(CO)₅ vapors in the presence of oxygen. The as synthesized samples were thermally treated at different temperatures between 150 – 550 °C for 2 hours and their morpho-structural properties were investigated. Furthermore, a treatment at 400 °C in NH₃ environment were also performed in order to induce a superficial nitridation of iron oxide NPs. XRD, TGA, XPS, EDX, DLS, TEM and magnetic analyses were performed on both the as synthesized and the treated ones. As a result, it was observed the consolidation of maghemite phase with increasing temperature up to 400 °C with a minimal increasing of crystalline dimension between (7.4 – 30.35 nm). The treatments at temperature higher than 450 °C suggest the solid phase transition from γ-Fe₂O₃ to α-Fe₂O₃ crystalline structure followed by a significant increasing in crystalline dimension. Also, the aqueous NPs suspension having 0.5 g/l concentration were performed. It was observed in the DLS analysis that the suspensions show a spectacular high stability in time for those NPs treated at lower temperature. However, the suspensions become unstable when NPs treated at temperatures higher than 250 °C were used. TGA analysis performed in air shows different steps of mass decreasing associated with water desorption between 90-130 °C, followed by a sudden decrease in mass between 150-280 °C probably as a result of the functional groups disappearance for treatments above 250 °C. The XPS studies made for O 1s and C 1s zones indicate the presence of Fe-OH, C=O and C-O bonds and with treatments at higher temperature such bonds attributed to functional bonds suffer a progressive attenuation.

1. INTRODUCTION

Nanoparticles refers to particles with all three external dimensions between 1 and 100 nm. Their synthesis is a fundamental element of nanotechnology due to the ability to generate or interact with systems at nanoscale level. Also, nanoparticles have a high specific surface area comparing with bulk materials opening novel perspectives in many fields like medicine [1,2], electronics [3], energy [4], environmental remediation [5], defense [6] and nonlinear optics [7].

Laser pyrolysis [8,9] plays a vital role in modern research by enabling the synthesis of high-quality nanomaterials with tailored properties, facilitating advances across various scientific and industrial fields. Its efficiency, adaptability, and ability to minimize contamination make it an essential technique in the development of innovative materials and technologies [9].

Laser pyrolysis can facilitate the exploration of new phases and allotropes of materials, leading to the discovery of novel compounds with unique properties, and has an ability to create materials with controlled characteristics allows researchers to investigate the relationships between structure and properties at the nanoscale [10,11].

This is what we set out to do in this work, using as a sensitizer a compound with a low carbon content in the process of obtaining magnetic nanoparticles through laser pyrolysis [12,13], to obtain the most durable stability and the best magnetization possible.

Formic acid (HCOOH) is a simple carboxylic acid that has found various applications in the field of nanotechnology. Its unique chemical properties and ability to act as a reducing agent [14, 15] make it useful in several processes involved in the synthesis and manipulation of nanomaterials. This method has been studied for its ability to produce nanoparticles with controlled size and shape, which are important for various applications, including electronics [16,17], catalysis [18,19], and biomedical fields [20,21].

The iron oxide nanopowders with high magnetic susceptibility might be structured as magnetite (Fe_3O_4), maghemite ($\gamma\text{Fe}_2\text{O}_3$) or a combination of them. Such iron oxide nanoparticles at very low dimension become superparamagnetic at room temperature and also combined with a low toxic feature for living cell they become a serious candidate for magnetic diagnosis agents [22-24] and intracellular drug delivery applications [25,26].

2. MATERIALES AND METHODS

If we analyze the synthesis of iron oxide exclusively, we observe that the use of classical sensitizers, such as ethylene [27,28] or sulfur hexafluoride nanoparticles [29], tends to lead to their agglomeration. We also find that their ability to be suspended and stabilized decreases as the temperature rises. Therefore, we infer that utilizing sensitizers with a lower absorption coefficient could be beneficial from two perspectives: on one hand, it could reduce the impurities of iron oxide nanoparticles caused by elements in the sensitizer molecule, such as sulfur or fluorine, as well as the high temperatures at which this sensitizer might decompose. For this reason, for the laser with an emission wavelength of 9.25 μm , we tested the formic acid molecule as a sensitizer. It meets our requirements in terms of absorption coefficient and contains a relatively low amount of carbon in its composition, namely one carbon atom among the five atoms of this molecule.

The image shows a schematic of a laser-induced pyrolysis setup used in the synthesis of magnetic iron oxide nanopowders in the presence of formic acid vapor as a sensitizer. Because this precursor is in a liquid state, a flow of inert gas, namely Argon, is bubbled through it. This technique uses energy from a continuous wave CO_2 laser operating at a wavelength of 9.25 μm , which is transferred to the reactive precursors by means of excited formic acid molecules (following the absorption of laser energy), inducing a rapid heating of the $\text{Fe}(\text{CO})_5$ vapor entrained by argon in the presence of oxygen. The laser beam focused using a ZnSe lens has a diameter of 2 mm and passes through 2 ZnSe windows that are blown on the inside with an Argon flow. The laser beam intersects orthogonally the reactant/inert gas flow that is introduced into the reaction zone by means of two concentric nozzles. Through the first annular nozzle with a diameter of 14.2 mm, an argon flow of 2000 sccm is introduced, with the role of confining the mixture of reactant gases that come through the inner nozzle with a diameter of 3.1 mm. The reactant mixture is composed of iron pentacarbonyl and formic acid vapors that are transported by the corresponding argon flow that bubbles each liquid, but also an oxygen flow that acts as an oxidizing agent. The gas flow resulting from the decomposition, together with the inert gas and the nanoparticles resulting from the reaction zone are

attracted to the collector chamber equipped with a porous filter by the vacuum pump. In the area of the intersection of the reactant gases with the laser beam, the chemical decomposition of the compounds takes place, forming a suspended flame that emits a smoke of nanoparticles.

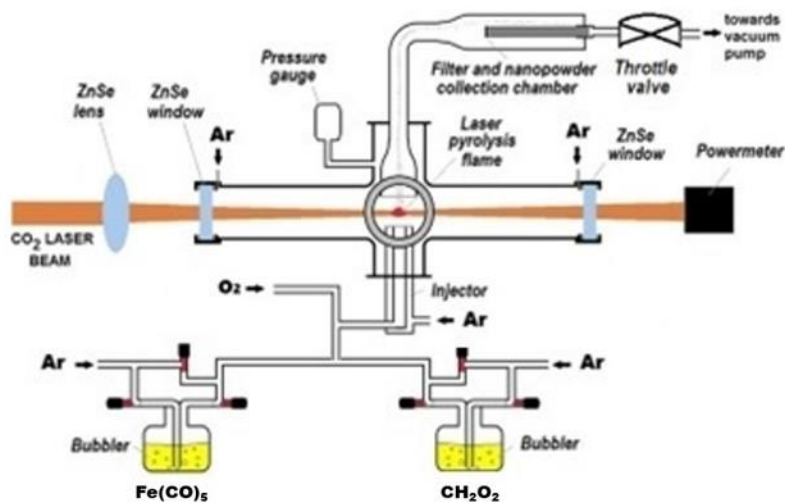


Fig. 1 - Experimental set-up of the laser pyrolysis technique for synthesizing iron oxide NPs using formic acid as sensitizer

The resulting nanoparticles were analyzed for their phase composition and crystallinity by X-ray diffraction (XRD) with a PANalytical X'Pert MPD theta-theta X-ray diffraction apparatus (Malvern Panalytical Ltd., Malvern, UK) with a Cu K α source (1.5418 Å). The Sherrer equation was used to perform evaluation of crystallite sizes of the NPs; in this case, a value of $k = 0.9$ for the shape factor was employed [26]. Elemental evaluation was performed using X-ray photoelectron spectroscopy (XPS) and energy-dispersive X-ray spectroscopy (EDS) analysis. X-ray photoelectron spectroscopy (XPS) employed an ESCALAB Xi+ X-ray Photoelectron Spectrometer Microprobe from Thermo Fisher Scientific Inc (Waltham, MA, USA) apparatus with an Al K α radiation source ($h\nu = 1486.2$ eV). The energy reference used was C 1s level (284.4 eV). 'Average' software, version 5.978, was employed for the identification of superficial chemical compositions and oxidation states. For the EDS investigations, the powders were hand-pressed and fixed onto copper foils, and the analysis was performed using the EDAX detector attached on a FEI Quanta Inspect S Scanning Electron Microscope (SEM) at 10 kV accelerating voltage (Thermo Fisher Scientific Inc. Waltham, MA, USA).

To investigate the particles size, morphology, and crystallinity degree, as well as to check the purity and chemical homogeneity of the samples, scanning electron microscopy (FE-SEM), transmission electron microscopy (TEM), and high resolution transmission electron microscopy (HR-TEM) coupled with selected area diffraction (SAED) and energy dispersive X-ray spectroscopy (EDX) analyses were performed using a high-resolution FEI QUANTA INSPECT F Scanning Electron Microscope with a field emission gun of 1.2 nm resolution and an EDX spectrometer with a Mn-K α resolution of 133 eV (Thermo Fisher Scientific, Waltham, MA, USA) and a TITAN THEMIS ultra-high resolution electron microscope 9 (Thermo Fisher Scientific, Waltham, MA, USA)

The magnetization of the samples was measured with Vibrating Sample Magnetometry (VSM) at room temperature using an ADE Technologies VSM880 magnetometer (Lowell, MA, USA). Thermogravimetry analysis was performed employing a Thermogravimetric Analysis/ Single Differential Thermal

Analysis (TGA/SDTA) Mettler Toledo apparatus, Greifensee, Switzerland. The measurements were attained in air, with a heating rate of 5 °C/min, from 25 °C up to 1000 °C.

3. RESULTS AND DISCUSSION

A very valuable analysis for identifying the crystalline phases of nanoparticles or materials in general is X-ray diffraction. Mainly for reading the crystalline phases a source is used that is monochromatic, that is, it has the same associated wavelength. In the case of materials analyzed with X-rays, we will use sources that emit in a wavelength close to the distances between atoms. If the distances between atoms are between 1 and 3 Å, one of the useful radiations for X-ray diffraction analysis is the source that emits on the copper $k\alpha$ length, namely 1.54 Å. This was also used in the case of our freshly synthesized nanoparticles. These are presented in the black curve in the graph on the left and the sample heat-treated at different temperatures in air. On the right is presented the spectrum of the raw sample but also treated at 400 °C in an ammonia atmosphere.

The size of the nanoparticles was calculated from the full width at half maximum (FWHM) using the Scherrer equation.

Following the thermal treatments, a high degree of crystallinity (average ordered size) and a phase change of iron are observed with increasing temperature in the atmosphere, namely: maghemite in the samples treated at 150-400 °C, a mixture of maghemite/hematite in the sample treated at 450 °C, the transition being made gradually up to the temperature of 500 °C and the hematite phase in the sample treated at 550 °C although the maghemite peaks do not disappear completely. Some peaks are replaced, but do not disappear (for example peaks (220) and (111)).

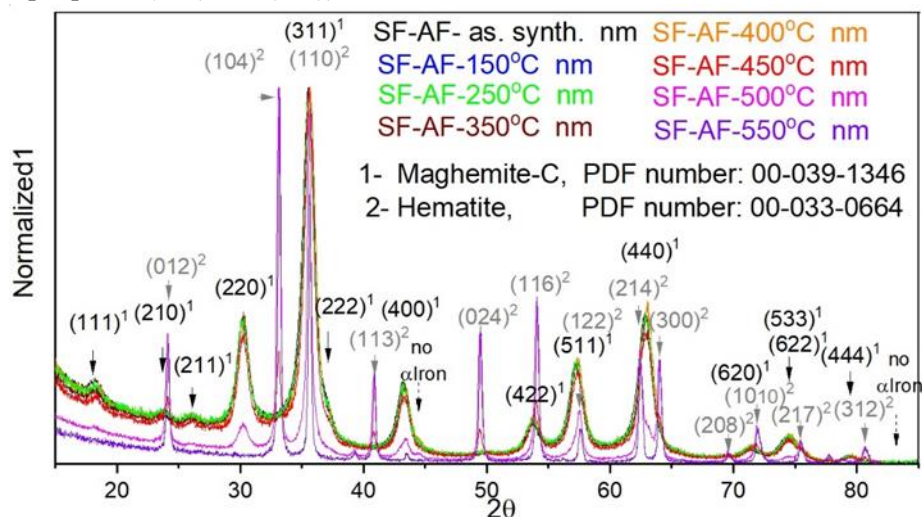


Fig. 2 - Stacked X-ray diffractograms for the iron oxide NPs attained heat-treated at different temperatures in air

In the sample treated in the ammonia atmosphere, additional peaks appear to the maghemite and magnetite phases, peaks that are attributed to the two iron nitride phases indicated in the figure with blue and green arrows. In the two heat treatments at 400 °C, we observe an increase in crystallite size of the maghemite phase, from 8.6 -30 nm in air atmosphere and from 7 nm in the raw sample to 30 nm in the sample heat treated in ammonia atmosphere. Also, 2 types of nitrides appear, although the maghemite/magnetite phase remains the majority.

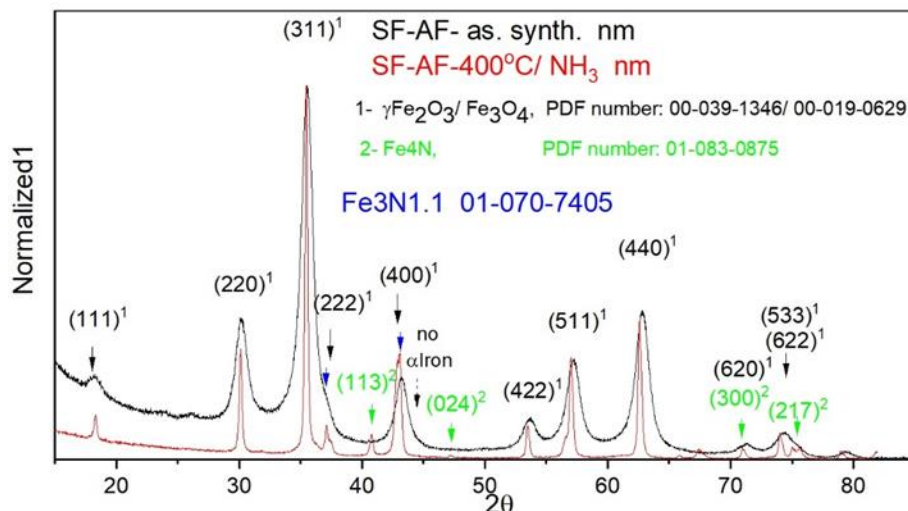


Fig. 3 - X-ray diffractograms of raw sample and sample treated in the ammonia atmosphere

A very interesting analysis and related to XRD, is the X-ray Photoelectron Spectroscopy analysis in which we irradiate our material with a monochromatic X-ray beam. As a result of the interaction of matter with X-rays, photoelectrons are produced and we analyze the kinetic energy of these photoelectrons. They retain in the received kinetic energy the trace of the interaction that the elements had between them. For example, we can identify after this loss of kinetic energy if the electrons come from a certain element or another such as Carbon, oxygen, or iron in our case, but in addition we can see from this positioning of the energy loss what bonds these elements form between them. In the spectra in the image, the intensity of the emitted photoelectron beam is presented, we identify by the positioning of the maxima what elements we have in the structure.

If we enter inside each peak positioned as we saw in the first graph in certain areas, we will be able to identify the type of bond that this element makes. We have for example the peaks from the active zone C1s, O1s or from the active zone of iron. In the case of oxygen, we identify what types of bonds it makes with Fe or bonds of the type of functional groups of the OH type. As you can see in the case of the raw sample and that of the sample treated at lower temperatures, the functional groups stand out now we will see that they generate a very good stability in water.

The XPS survey spectra of the SF-AF1 samples reveal the presence of C 1s, Fe 2p, and O 1s signals for all conditions. Notably, the sample treated at 400 °C in NH₃ atmosphere (SF-AF1-T400NH₃) exhibits an additional N 1s signal, indicating successful nitrogen doping. The atomic percentage of nitrogen was estimated to be 4.68 at%, confirming efficient incorporation of nitrogen species during the thermal treatment under ammonia. The high-resolution N 1s spectrum of the SF-AF1-T400NH₃ sample confirms the presence of nitrogen species incorporated into the carbon structure. Deconvolution reveals three distinct components centered at 396.7 eV, 398.0 eV, and 399.8 eV, corresponding to metal–N bonds, pyridinic-N, and pyrrolic-N species, respectively. These nitrogen configurations are known to contribute to improved catalytic activity in various electrochemical applications.

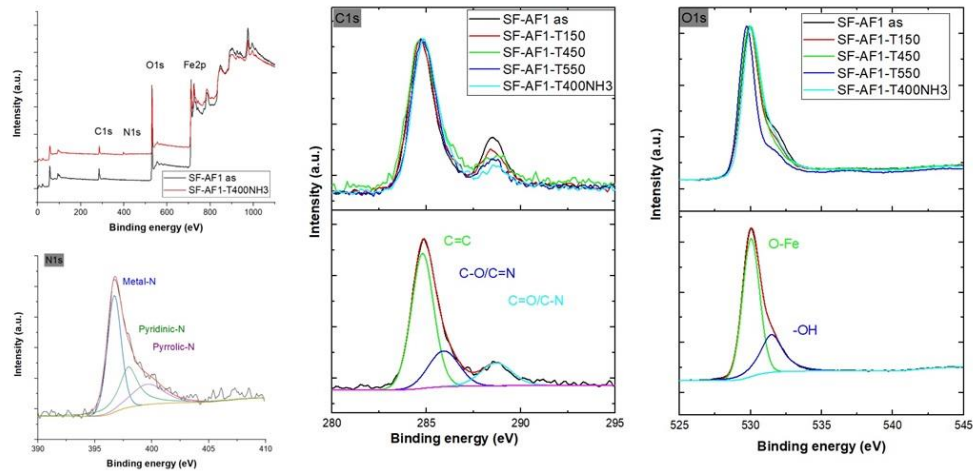


Fig. 4 - The XPS spectra of treated samples

The high-resolution C 1s spectra show the comparison between all samples (top) and the deconvoluted spectrum of SF-AF1-T400NH₃ (bottom). Upon heating in air up to 450 °C, the intensity of the peak assigned to C=O/C-N (~288.7 eV) decreases, while the peak corresponding to C-O/C=N (~285.9 eV) increases, suggesting partial reduction and chemical rearrangement of oxygenated surface functionalities. At 550 °C, both contributions are reduced. In contrast, the NH₃-treated sample displays diminished intensities in both the C-O/C=N and C=O/C-N regions, implying effective nitrogen incorporation and partial removal of oxygenated groups.

The O 1s spectra were deconvoluted into two main contributions: a peak at ~530 eV attributed to O-Fe bonds and a higher binding energy peak at ~531.5 eV corresponding to surface hydroxyl groups (-OH). Heating in air leads to a gradual decrease in the -OH component, while treatment in NH₃ atmosphere enhances the -OH signal, likely due to surface interactions with NH₃-derived species.

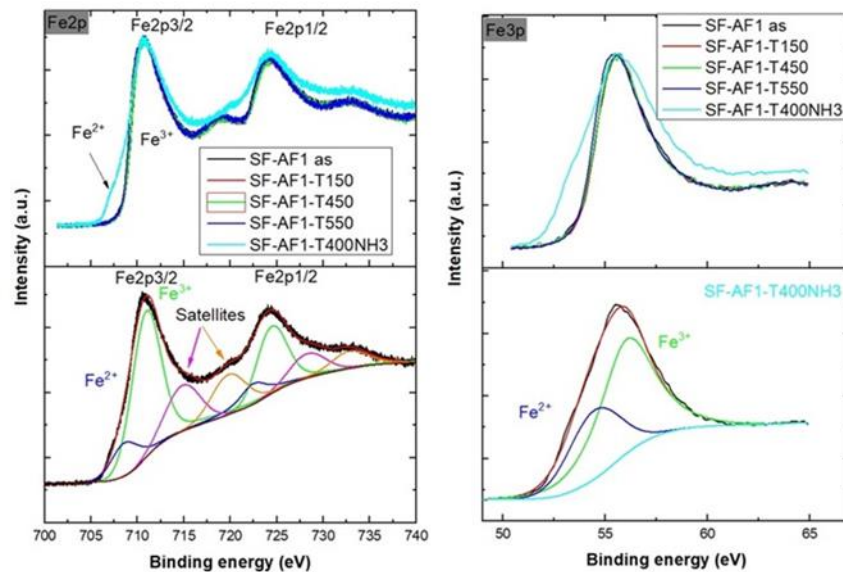


Fig. 5 - Fe 2p and Fe 3p spectra of treated samples

The Fe 2p and Fe 3p spectra were recorded to investigate the oxidation states of iron in the SF-AF1 samples. The use of both Fe 2p and Fe 3p regions provides a more reliable evaluation of the chemical state of Fe species, especially considering the multiple splitting and satellite features typically observed in Fe 2p spectra, which may complicate peak fitting. In contrast, the Fe 3p spectrum is simpler, providing complementary information to support the interpretation of Fe oxidation states. In the samples treated in air, the XPS analysis indicates the presence of Fe³⁺ as the predominant oxidation state, even at high temperatures such as 550 °C. This is attributed to the oxidative environment that stabilizes ferric species. In an oxygen-rich atmosphere, iron is readily oxidized, and the thermal energy promotes the formation of stable Fe³⁺ oxides such as Fe₂O₃, which are thermodynamically favored. In contrast, the sample treated at 400 °C in NH₃ atmosphere exhibits a clear contribution from both Fe³⁺ and Fe²⁺ species. The appearance of Fe²⁺ is due to the reductive nature of the ammonia atmosphere. NH₃ can act as a reducing agent at elevated temperatures, leading to the partial reduction of Fe³⁺ to Fe²⁺.

This transformation reflects changes in the local coordination environment and may play a crucial role in the development of catalytically active Fe–N–C structures, which are known for their activity in oxygen reduction reactions. Therefore, the combined analysis of both Fe 2p and Fe 3p spectra allows for an accurate and comprehensive assessment of the iron redox behavior, essential for understanding the catalytic properties of the materials synthesized under different thermal and atmospheric conditions.

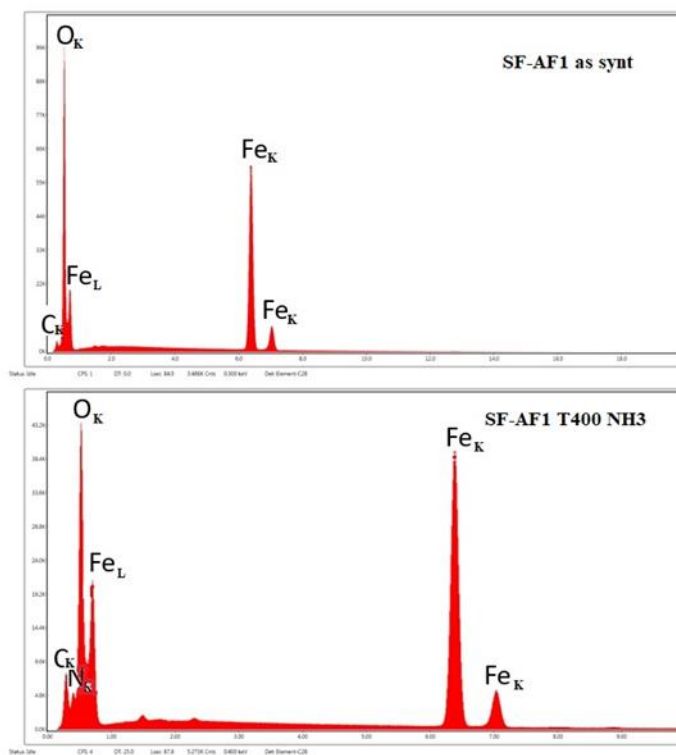


Fig. 6 - EDAX spectra

A very important analysis in terms of evaluating the elemental composition is EDAX. This happens by irradiating our nanometric material with a monochromatic electron beam with a constant kinetic energy generated in a Scanning Electron Microscope. Following the interaction with the matter, electrons are extracted from the deep levels and these levels will capture peripheral electrons, releasing a characteristic radiation of the respective element. More precisely, the energy of the emitted X-ray radiation is a label of

the respective atom. We can identify the elemental composition of our material by the intensity of this X-ray radiation present. For example, in the image xxx we observe the presence of carbon, oxygen and iron. This is identified in two positions: once when we talk about the deep levels of type L 2p or when we talk about the deep levels of 1s (Fek).

Table 1

Elemental composition evaluation by EDS for synthesized NPs with formic acid as sensitizer

| Sample | Fe [%at.] | O [% at.] | C [% at.] | N [% at.] |
|--------------------------------|-----------|-----------|-----------|-----------|
| SF - AF1 | 41.45 | 58.13 | 0.43 | - |
| SF - AF1 T150° | 42.64 | 56.89 | 0.47 | - |
| SF - AF1 T250° | 45.06 | 54.79 | 0.15 | - |
| SF - AF1 T350° | 43.44 | 55.04 | 1.52 | - |
| SF - AF1 T400° | 44.46 | 55.19 | 0.36 | - |
| SF - AF1 T450° | 44.98 | 54.4 | 0.62 | - |
| SF - AF1 T500° | 42.67 | 57.33 | 0 | - |
| SF - AF1 T550° | 44.72 | 55.28 | 0 | - |
| SF - AF1 T400° NH ₃ | 40.35 | 43.22 | 10.19 | 6.24 |

The freshly synthesized nanoparticles are analyzed thermogravimetrically. TGA analysis is an analysis in which we highlight the mass losses with the heating of the sample. The heating is done in a uniform yield in terms of the heating regime, in our case being 5 °/minute between room temperature and 1000 °C.

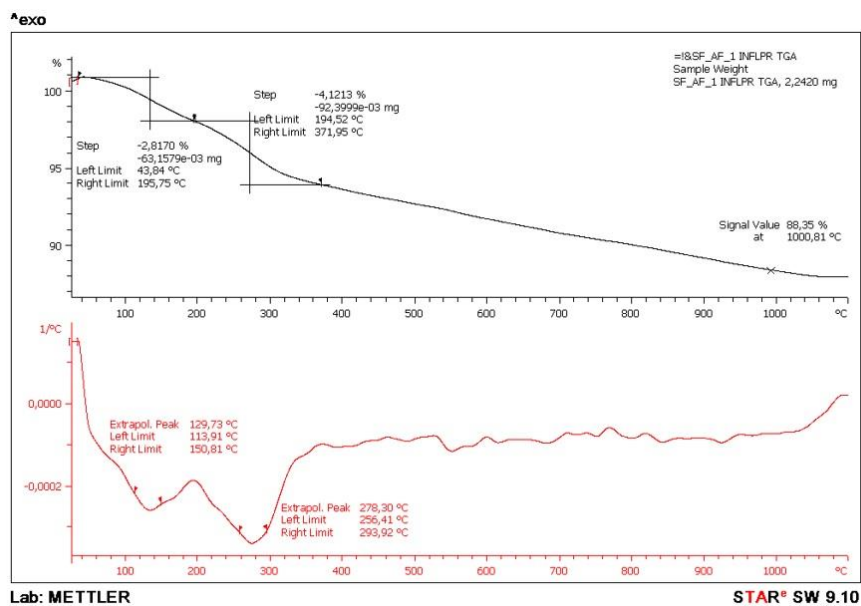


Fig. 7 - TGA thermograms for sample as synthesized

The upper curve, the black one, indicates a slight continuous mass decrease highlighting different decrease thresholds. Thus, a first decrease passage is in the range up to 150 °C with an inflection point at 130 °C, which is usually attributed to the processes of elimination of physically or chemo-absorbed water molecules. After the temperature of 150 °C, the mass loss continues in a somewhat more pronounced regime and we consider that this is due, as seen from the previously presented analyses, to the disappearance of some functional groups formed on the surface of these nanoparticles. As a rule, functional groups, if they

also have a molar character, are useful in the case where the nanoparticles will be dispersed in molar liquids such as water. Thus, we consider that the second passage between 256 – 300 °C with an inflection point centered at 280 °C is due to the loss of these functional groups. Due to the presence of carbon in both the iron precursor and the sensitizer, there are still carbon-based functional groups on the surface of the synthesized iron oxide nanoparticles. These functional groups or superficial carbon islands, obviously at higher temperatures become reactive and can produce oxidation phenomena, and the carbon transforming into carbon dioxide, results in a new mass loss in the analyzed particles. We consider that the third, much less pronounced mass loss threshold, the one that has an inflection point at 550 °C, is due to the loss of these areas where carbon is present superficially on the surface of the respective nanoparticles. It is also possible that the recrystallization process generated by the phase transition from the magnetic iron oxide phase to the non-magnetic phase called hematite is accompanied by a more pronounced loss of these carbon-based functional groups.

TEM image of NPs for the as-synthesized sample is presented in the fig.8. In the SAED image, the x-ray diffraction rings are observed in which the interplanar distances specific to maghemite are identified. As shown in the right side of the raw sample consists of small agglomerated nanoparticles. The mean size diameter of particles is approx. 7.3 nm. HR-TEM analyses evidence the presence of spherical aggregates of about 150 nm diameter formed from small polyhedral-shaped nanoparticles.

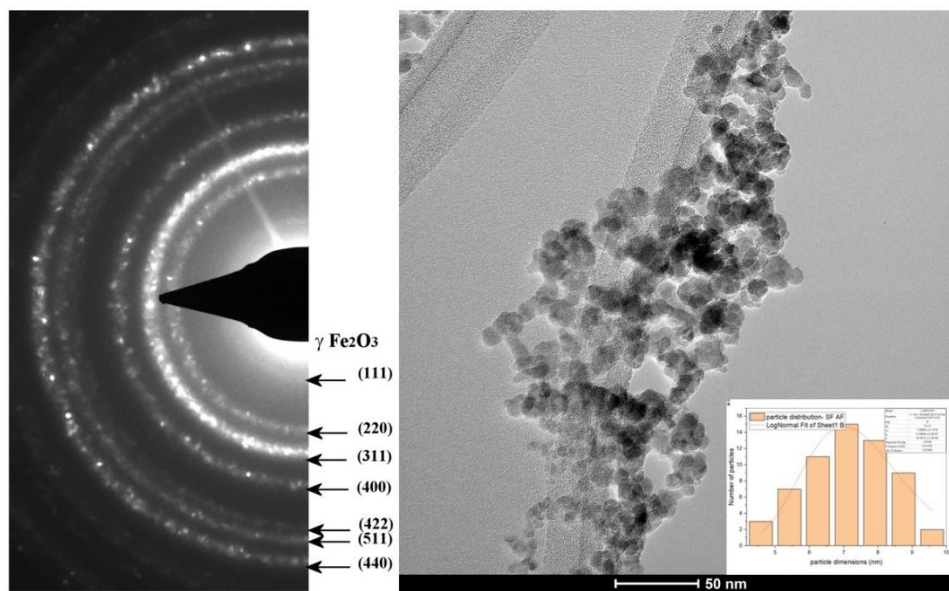


Fig. 8 - SAED image in the left part and in right TEM image for raw sample

Our nanoparticles can be used as fluids with biomedical applications or in energy transfer, or as ink. To evaluate the dispersion capacity of these nanoparticles we will use the Dynamic Light Scattering Measurement Device. This analysis is because the nanometric material being so fine, could exhibit Brownian motion when in a liquid. In our case, for the targeted applications we make concentrated suspensions. From the DLS analysis we can find out what the dimensional organization of the nanoparticle agglomerates is.

Also, a concentration study of the nanoparticles obtained by laser pyrolysis using formic acid as a sensitizer was carried out, and it was observed that in the case of all concentrations the suspensions are extremely stable over time with dimensions ranging between 84-107 nm, with an average polydispersity index of 0.35.

Table 2

Concentration study of iron oxide nanoparticles dispersed in distilled water

| Samples | Size 5 min | | 24 H | |
|----------------|------------|-------|-----------|-------|
| | Size [nm] | PI | Size [nm] | PI |
| SF-AF1 0.5 g/l | 91.3 | 0.396 | 106.0 | 0.385 |
| SF-AF1 1 g/l | 94.3 | 0.407 | 85.5 | 0.317 |
| SF-AF1 2.5 g/l | 93.8 | 0.358 | 106.3 | 0.407 |
| SF-AF1 5 g/l | 84.8 | 0.338 | 80.8 | 0.248 |
| SF-AF1 10 g/l | 107.8 | 0.442 | 92.2 | 0.385 |

In the case of heat-treated samples, aqueous suspensions of nanoparticles with a concentration of 0.5 g/l were made. In DLS analyses, it was observed that the suspensions show high stability over time for those nanoparticles treated at lower temperatures, such as those at 150 and 250 °C. While the suspensions become unstable when nanoparticles treated at temperatures higher than 250 °C were used. In the case of the sample treated in an ammonia atmosphere, the sample was unstable, due to the iron nitride phase which is not stable in an aqueous environment.

Table 3

Variation in particle size dispersed in distilled water

| Samples | Size 5 min | | 24 H | |
|-------------------------------|------------|-------|-----------|-------|
| | Size [nm] | PI | Size [nm] | PI |
| SF-AF1 | 91.3 | 0.396 | 106.0 | 0.385 |
| SF-AF1 T150 ° | 121.5 | 0.381 | 118.6 | 0.422 |
| SF-AF1 T250 ° | 219.3 | 0.409 | 200.9 | 0.469 |
| SF-AF1 T350 ° | 3684.3 | 0.425 | - | - |
| SF-AF1 T400 ° | 6216.2 | 0.741 | - | - |
| SF-AF1 T450 ° | 4212.2 | 0.348 | - | - |
| SF-AF1 T500 ° | 2398.2 | 0.686 | - | - |
| SF-AF1 T550 ° | 2227.1 | 0.367 | 225.6 | 0.389 |
| SF-AF1 T400 ° NH ₃ | 5472.2 | 0.289 | - | - |

We also observe that although in the case of the raw sample we have a positive Zeta potential, it changes its sign due to the presence of carbon inside the iron crystal lattice. The decrease in the Zeta potential can be interpreted by the appearance of basic groups induced by the ammonia treatment (bonds (Fe-O-) appear).

Table 4

Zeta Potential of raw sample and treated in NH₃ atmosphere sample

| Sample | Zeta potential [mV] |
|-------------------------------|---------------------|
| SF-AF1 | 50.6 |
| SF-AF1 T400 ° NH ₃ | -58 |

Following magnetic analyses, it is observed that with heat treatment the saturation magnetization increases up to 56 emu/gram and all samples show a superparamagnetic character because there is no coercive field. The magnetic properties are influenced by the size of the nano crystallites.

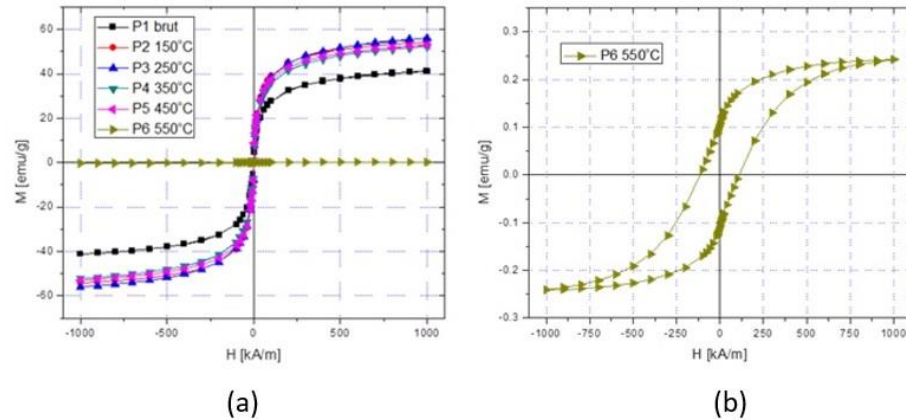


Fig. 9 - Hysteresis loops for samples treated in air atmosphere (a) up to and including 450 °C and (b) sample treated 550 °C

In figure 9, hysteresis loops are graphical representations of the relationship between the magnetic field and the magnetization of a material. They are vital for understanding the magnetic properties of different materials, particularly ferromagnetic materials. In this case it can be observed that the hysteresis loop for samples treated in air will exhibit a typical “S” shape. The width of the loop indicates the coercivity (the resistance to demagnetization) and the area within it represents energy loss due to magnetic hysteresis, the superparamagnetic behavior.

It can be observed a saturation magnetization value where the curve flattens, indicating that further increases in the magnetic field do not result in increased magnetization. After the external field is removed, may retain some magnetization, known as remanent magnetization, which in the case of the samples treated up to and including 450 °C is equal to zero unlike the sample treated at 550 °C.

Table 5.

Saturation magnetization of samples treated in air atmosphere

| Samples | Msat@1MA/m [emu/g] | Mr [emu/g] | Hc [kA/m] |
|--------------|-----------------------|---------------|--------------|
| SF-AF1-brut | 41.0 | 0 | 0 |
| SF-AF1-150°C | 54.0 | 0 | 0 |
| SF-AF1-250°C | 55.9 | 0 | 0 |
| SF-AF1-350°C | 52.1 | 0 | 0 |
| SF-AF1-450°C | 52.8 | 0 | 0 |
| SF-AF1-550°C | 0.24 | 0.11 | 113 |

The hysteresis loop can be influenced by factors such as oxidation, grain size, and the presence of impurities due to the air treatment. In the case of samples treated at temperatures lower than 450 °C, it is observed that we find the maghemite/magnetite phase, and in the case of the sample treated at 550 °C, it is observed that the material is hematite. Analyzing the differences between the two will help understand how treatment conditions influence magnetic properties, valuable in applications such as magnetic materials and devices.

4. CONCLUSIONS

Laser pyrolysis facilitates the obtaining of iron oxide nanoparticles with very low dimensions, a reduced dimensional dispersion, optimum crystallinity and in quite large quantities: a couple of grams per hour with an experimental set-up that have the potential to be scaled-up for industrial needs.

For better stability in aqueous environments, it was desired to use precursors with a low percentage of carbon, and formic acid proved to be a very good one. The use of formic acid facilitates the formation of functional groups on the surface of the particles and gives the nanoparticles excellent stability in aqueous environments without surfactants.

The combined analysis of both Fe 2p and Fe 3p spectra allows for an accurate and comprehensive assessment of the iron oxidation state in these nanoparticles synthesized under different thermal and environmental conditions.

Following thermogravimetric analyses, significant decreases in the sample mass are observed, which are explained by the disappearance of volatile products from the sample, but also of the functional groups on the surface of the nanoparticles. Also, a crystalline rearrangement or transformation of their structures occurs with the heating of the samples in air or ammonia.

Following the treatment in the ammonia atmosphere, it is observed that the nitrogen peak is found in the sample structure at EDX, signaling that the doping was successful. Following the heat treatment in the ammonia atmosphere, two distinct iron nitride phases appear.

The powders were treated at different temperatures, and the influence this has on their structural and elemental composition was also analyzed. With the increase in temperature, the crystallinity of the nanoparticles is also enhanced, and are structured as a mixture of maghemite and magnetite, the crystallite dimension also slightly increasing. The stability of iron oxide nanoparticles synthesized with formic acid does not depend on the concentration of nanoparticles and results range between 84-107 nm, and after 24 hours their stability changes only very slightly.

The characteristics of the magnetic nanoparticles were evaluated at room temperature, showing their predominantly superparamagnetic character. The saturation magnetization and the (very low) coercive field decrease with crystallite size: from approximately 55 emu/g to less than 10 emu/g.

Thermogravimetric analysis indicates a significant weight loss between 25 and 1000 °C, with a zone between 114 – 151 °C and the second with temperatures between 256 – 295 °C with maxima at 130 and 279 °C. A phase change is also seen at temperatures of 550 °C.

Either as morpho-structural and magnetic properties or as components in aqueous suspensions, our samples present promising features for future applications, such as hyperthermia, drug delivery, and heat transfer agents. The decrease in Zeta Potential can be interpreted by the appearance of basic groups induced by the ammonia treatment.

The hysteresis loops from both samples provide valuable insights into their magnetic behavior. The samples treated up to and including 450 °C could exhibit superparamagnetic behavior due to oxidation and other environmental factors, while the one treated at 550 °C will likely show enhancements due to thermal effects on its microstructure. Analyzing the differences between the two will help understand how treatment conditions influence magnetic properties, valuable in applications such as magnetic materials and devices.

5. ACKNOWLEDGEMENTS

This research was supported (or financed) by Romanian Ministry of Education and Research, under Romanian National Nucleus Program LAPLAS VII – contract no. 30N/2023 and Project 121PED/2025.

The work of VMS was supported by the RA-TB/CFATR/LMF multiannual research program 2021–2025.

REFERENCES

1. T.M. Joseph, D. Kar Mahapatra, A. Esmacili, L. Piszczyk, M.S. Hasanin, M. Kattali, J. Haponiuk, S. Thomas, *Nanoparticles* **13**, 574 (2023).
2. G. Tabacchi, I. Armenia, G. Bernardini, N. Masciocchi, A. Guagliardi, E. Fois, *ACS Applied Nano Materials* **6** (14), 12914-12921 (2023).
3. M. Harshada, K. Yuvraj, S.S. Patil, *IJAENT* **4**, 6 (2021).
4. R. Raj, R.Verma, J. Singh, *Nanomaterials for Energy Storage Applications, Bioenergy Research: Integrative Solution for Existing Roadblock* **7**, 135-156, (2021).
5. F.D. Guerra, M.F. Attia MF, D.C. Whitehead, F. Alexis, *Molecules* **18**, 23(7), 1760 (2018).
6. Z. Foltynowicz, B. Czajka, A. Maranda, L. Wachowski, *High Energy Materials* **12** (1), 17 – 36 (2020).
7. A. Guzmán-Barraza, J.G. Ortega-Mendoza, A. Padilla-Vivanco, M.L.A. Carrasco, N.R. Silva-González, P. Zaca-Morán, E.V.G. Ramírez, *Result in Optics* **14**, 100590 (2024).
8. C. Spreafico, D. Russo, R. Degl' Innocenti, *J. of Intelligent Manufacturing* **33** (2), 353-385 (2022).
9. N. Herlin-Boime, M. Mayne-L' Hermite, C. Reynaud, C, *Ann. Chim. - Sci. Mat* **31** (3), 295-315 (2006).
10. F. Dumitrache, A. Criveanu, I. Lungu, C. Fleaca, L. Gavrilă-Florescu, I. Morjan, I. Stamatina, A. Balan, V.Socoliuc, B. Vasile, *Coatings* **15** (2), 234 (2025).
11. E. Goncarenco, I.P. Morjan, C. Fleaca, E. Dutu, A. Criveanu, C. Viespe, A.C. Galca, A.V. Maraloiu, M.S. Stan, C.I. Fort, M. Scarisoreanu, *Sustainability* **16** (7), 2904 (2024).
12. G. Schinteie, V. Kuncser, P. Palade, F. Dumitrache, R. Alexandrescu, I. Morjan, G. Filoti, G, *J. Alloys Compd.* **564**, 27-34 (2013).
13. I.I. Lungu, E. Andronescu, F. Dumitrache, L. Gavrilă-Florescu, I. Morjan, A.M. Banici, C. Fleaca, A. Criveanu, G. Prodan, *University Politehnica of Bucharest Scientific Bulletin Series B- Chemistry and Materials Science* **86** (1) 109-118 (2024).
14. M.A. Fouad, F. Ferretti, F. Ragaini, *J. Org. Chem.* **88** (8) 5108-5117 (2023).
15. O. Mokhtari, F. Conti, S.K. Bhogaraju, M. Meier, Markus, H. Schweigart, U. Tetzlaff, G. Elger, G; *New J. Chem.* **43** (26) 10227-10231 (2019).
16. S.S. Liu, L. Yang, J.B. Xin, X.C. Lv, Y. Chen, Y. Liu, *J. Mater. Sci. - Mater. Electron* **35** (22), 1493 (2024).
17. Y. Meng, Y. Xu, R.H. Gao, X.H. Wang, X.J. Chen, S. Huang, K. Wei, D.H. Wang, H.B. Yin, K. Takeuchi, T. Suga, F.W. Mu, X.Y. Liu, *J. Mater. Sci. - Mater. Electron* **33** (5), 2582-2589 (2022).
18. M. Al-Naji, J. Van Aelst, Y.H. Liao, M. d'Hullian, Z.P. Tian, C.G. Wang, R. Gläser, B.F. Sels, *Green Chem.* **22** (4), 1171-118 (2020).
19. P. Kankla, T. Butburee, N. Chanlek, S. Sattayaporn, P. Luksirikul, *Top. Catal.* **66** (19-20), 1608-1618 (2023).
20. Y.N. Jo, I.C. Um, *Int. J. Biol. Macromol.* **78**, 287-295 (2015).
21. M.T. Isa, A.Y. Abdulkarim, A. Bello, T.K. Bello, Y. Adamu, *J. Biomater. Appl.* **38** (10), 1036-1057, (2024).
22. J.J. Lai, Z.Z. Luo, L.T. Chen, Z.B. Wu, *Sci. Prog.* **107** (1), 1–18 (2024).
23. S. Salatin, M. Farhoudi, S. Sadigh-Eteghad, J. Mahmoudi, *Expert Opinion on Drug Delivery* **21** (4), 521-535 (2024).
24. B. Govindan, M.A. Sabri, A. Hai, F. Banat, M. Abu Haija, *Pharmaceutics* **15** (3), 868 (2023).
25. N.T.T. Nguyen, T.T.T.; Nguyen, S.B. Ge, R.K. Liew, D.T.C. Nguyen, T.V. Tran, *Nanoscale Advances* **6** (7), 1800-1821 (2024).
26. N. Ejderyan, Y. Oz, R. Sanyal, A. Sanyal, *Biomacromolecules* **26** (3), 1555-1570 (2025).
27. C.T. Fleaca, I. Morjan, R. Alexandrescu, F. Dumitrache, I. Soare, L. Gavrilă-Florescu, F. Le Normand, A. Derory, *Appl. Surf. Sci.* **255** (10), 5386-5390 (2009).
28. C. Fleaca, F. Dumitrache, E. Dutu, C. Luculescu, A.M. Niculescu, A. Ilie, E. Vasile, *University Politehnica of Bucharest Scientific Bulletin Series B- Chemistry and Materials Science* **78** (2), 43-56 (2016).
29. F. Dumitrache, I.P. Morjan, E. Dutu, I. Morjan, C.T. Fleaca, M. Scarisoreanu, A. Ilie, M. Dumitru, C. Mihailescu, A. Smarandache, G. Prodan, G; "Zn/F-doped tin oxide nanoparticles synthesized by laser pyrolysis: structural and optical properties", *Beilstein Journal of Nanotechnology* **10**, 9-21 (2019).